JLab Program Advisory Committee Eleven Proposal Cover Sheet

This document must be received by close of business on ~~Wednesday, December 18, 1996 at:~~

Jefferson Lab
User Liaison Office, Mail Stop 12 B
12000 Jefferson Avenue
Newport News, VA 23606

(Choose one)

☑ **New Proposal Title:** Electroproduction of Hypernuclei in ^{3}He and ^{4}He

☐ **Update Experiment Number:**

☐ **Letter-of-Intent Title:**

Contact Person

Name: Teijiro Saito
Institution: Laboratory of Nuclear Science, Tohoku University
Address: 1-2-1, Mikamine, Taihaku-ku
Address:
City, State ZIP/Country: Sendai 982, JAPAN
Phone: 022-743-3429 **FAX:** 022-743-3401
E-Mail › Internet: saito@thrlm1.lns.tohoku.ac.jp

Experimental Hall: A **Days Requested for Approval:** 34

Jefferson Lab Use Only

Receipt Date: 6/26/97 PR 97-003

By: gn

BEAM REQUIREMENTS LIST

JLab Proposal No.: _____ Date: _____

Hall: A Anticipated Run Date: _____ PAC Approved Days: _____

Spokesperson: Teijiro Saito Hall Liaison: _____
Phone: 022-743-3429
E-mail: saito@thk.lns.tohoku.ac.jp

List all combinations of anticipated targets and beam conditions required to execute the experiment. (This list will form the primary basis for the Radiation Safety Assesment Document (RSAD) calculations that must be performed for each experiment.)

Condition No.	Beam Energy (MeV)	Mean Beam Current (μA)	Polarization and Other Special Requirements (e.g., time structure)	Target Material (use multiple rows for complex targets — e.g., w/windows)	Material Thickness (mg/cm²)	Est. Beam-On Time for Cond. No. (hours)
1	3,000	50		solid target calib. & checkout		100
2	3,000	50		cryogenic ^{4}He	750	350
3	3,000	50		cryogenic ^{3}He	930	350

The beam energies, E_{Beam}, available are: $E_{Beam} = N \times E_{Linac}$ where N = 1, 2, 3, 4, or 5. E_{Linac} = 800 MeV, i.e., available E_{Beam} are 800, 1600, 2400, 3200, and 4000 MeV. Other energies should be arranged with the Hall Leader before listing.

LAB RESOURCES REQUIREMENTS LIST

CEBAF Proposal No.: _____ Date: _____
(For CEBAF User Liaison Office use only.)

List below significant resources — both equipment and human — that you are requesting *from CEBAF* in support of mounting and executing the proposed experiment. Do not include items that will be routinely supplied to all running experiments, such as the base equipment for the hall and technical support for routine operation, installation, and maintenance.

***Major Installations** (either your equip. or new equip. requested from CEBAF)*

We must install
a) two super conducting septum magnets
b) cryogenic system for the septum magnets
c) septum scattering chamber
d) exit beam pipe
e) one correction coil
and support structures for them.

New Support Structures: _____

Data Acquisition/Reduction

Computing Resources: _____

New Software: _____

Major Equipment

Magnets _____

Power Supplies _____

Targets cryogenic ^3He, ^4He

Detectors _____

Electronics _____

Computer Hardware _____

Other _____

Other

HAZARD IDENTIFICATION CHECKLIST

CEBAF Experiment: _____ Date: _____

Check all items for which there is an anticipated need—do not check items that are part of the CEBAF standard experiment (HRSE, HRSH, CLAS, HMS, SOS in standard configurations).

Cryogenics
- _____ beamline magnets
- ✓ analysis magnets
- ✓ target
- _____ drift chambers
- _____ other

Electrical Equipment
- _____ cryo/electrical devices
- _____ capacitor banks
- _____ high voltage
- _____ exposed equipment

Radioactive/Hazardous Materials
List any radioactive or hazadorous/ toxic materials planned for use:
_____
_____

Pressure Vessels
- _____ inside diameter
- _____ operating pressure
- _____ window material
- _____ window thickness

Flammable Gas or Liquids
(incl. target)
type: _____
flow rate: _____
capacity: _____

Other Target Materials
- ___ Beryllium (Be)
- ___ Lithium (Li)
- ___ Mercury (Hg)
- ___ Lead (Pb)
- ___ Tungsten (W)
- ___ Uranium (U)
- ___ Other (list below)

_____
_____

Vacuum Vessels
- _____ inside diameter
- _____ operating pressure
- _____ window material
- _____ window thickness

Radioactive Sources
- _____ permanent installation
- _____ temporary use

type: _____
strength: _____

Large Mech. Structure/System
- _____ lifting devices
- _____ motion controllers
- _____ scaffolding or elevated platforms
- _____ other

Lasers
type: _____
wattage: _____
class: _____

Installation
- _____ permanent
- _____ temporary

Use
- _____ calibration
- _____ alignment

Hazardous Materials
- ___ cyanide plating materials
- ___ scintillation oil (from)
- ___ PCBs
- ___ methane
- ___ TMAE
- ___ TEA
- ___ photographic developers
- ___ other (list below)

_____
_____
_____

Notes:
_____
_____
_____
_____
_____
_____

JLab PROPOSAL

Electroproduction of Hypernuclei in ^{3}He and ^{4}He

T. Saito(Spokesperson and Contact person), J. Kasagi, O. Konno,
T. Terasawa(Spokesperson), H. Yamazaki
Laboratory of Nuclear Science, Tohoku University
K. Maeda, T. Nakagawa, T. Suda, H. Tsubota
Department of Physics, Tohoku University
S. Kato, H. Ueno
Department of Physics, Yamagata University
Y. Akaishi
Institute for Nuclear Study, University of Tokyo
S. Shinmura
Faculty of Engineering, Gifu University
S. Frullani, F. Garibaldi, M. Iodice, G.M. Urciuoli(Spokesperson)
Instituto Superiore di Sanita
R. de Leo
Bari Univesity
R. Perrino, A. Leone
INFN-Lecce
P. Markowitz(Spokesperson)
Florida International University
C.C. Chang
Maryland University
K. de Jager, J.P. Chen, J. Le Rose, A. Saha, B. Wojtsekhowski
Jefferson Laboratory
O.K. Baker
Hampton University
C. Perdrisat
Physics Department, College of William and Mary
D. Vina Punjabi
Department of Physics and Chemistry, Norfolk State University
M. Epstein
Physics Department, California State University
and
Hall A Collaboration

I. Abstract

We are interested in electroproduction of hypernuclei to investigate Λ and bound Σ hypernuclear states for the ^{3}H and ^{4}H nuclei. In this study angular distributions of the kaons at forward angles are measured to identify J^π of the hypernuclear states. In order to allow measurements at very forward angles, the septum magnets for the Hall A spectrometers are used. The proposed experiments will provide information on the Λ-N spin-spin interaction and bound Σ hypernuclei.

II. Introduction

Hypernuclear states have been studied by the (K^-, π^-), (π^+, K^+) and stopped K reactions. Each reaction has different characteristics. The (K^-, π^-) reaction at small angles is a process with small momentum transfer. In this case it preferentially populates substitutional hypernuclear states in which a nucleon is replaced by a Λ particle. This transition is characterized by an orbital angular momentum transfer of $\Delta L=0$. The (π^+, K^+) reaction favors the formation of high spin states due to large momentum transfer. The stopped K reaction is a special case of the (K^-, π^-) reaction where a kaon is captured at rest. In this reaction variety of hypernuclear states is populated by a sizable momentum transfer.

For the Λ hypernuclei up to ^{89}Y , the binding energies of the single particle states of the Λ were obtained by the (π^+, K^+) experiments at BNL[1]. On the other hand for the Σ hypernuclei, many candidates for narrow Σ states in the continuum in light nuclei have been found, but not confirmed as the Σ hypernuclei[2]. The first evidence of a bound Σ state for A = 4 was reported through the ^{4}He(K^-, π^-) reaction at rest[3]. Recently clear evidence of a bound Σ state for A=4 was observed in the (K^-, π^-) experiments at BNL[4]. The hypernuclear production so far reported have been done with an energy resolution of 2~3MeV. Thus, it is highly desirable to study the hypernuclear states by another probe with much higher resolution.

The (e, e' K^+) and (γ, K^+) reactions are expected to provide a useful alternative to the (π^+, K^+) and (K^-, π^-) reactions. The (e, e' K^+) reaction is similar to (π^+, K^+) reaction in regard to variable momentum transfer, but the former has some advantages for studying deeply-bound Λ orbits. The electrons are very weakly absorbed in compared with the pions. In addition the (e, e' K^+) reaction excites both natural and unnatural parity hypernuclear states with comparable strength. Many theoretical predictions have been

carried out for hypernuclear production by the (e, e' K^+) and (γ, K^+) reactions. Recently Shinmura[5] has calculated production cross sections of light Λ and Σ hypernuclei in the (e, e' K^+) reactions at around TJNAF energies. The results have shown that unnatural parity states and stretched states of hypernuclei are favorably excited because of dominant spin-flip amplitudes and large momentum transfer. No experimental data for electromagnetic production of hypernuclei have been reported up to the present. Recently a feasibility study of electroproduction of hypernuclei with the ^{12}C and ^{27}Al targets has been done at TJNAF[6].

We emphasize that the high resolution measurement of hypernuclear states produced in the (e, e' K^+) reaction on the ^3He and ^4He targets is a promising experiment. It will provide information on the Λ-N spin-spin interaction and the bound Σ hypernuclei. It will also provide a test of the capabilities of study of the deeply bound state in heavy nuclei. The (e, e' K^+) measurements are not feasible anywhere but TJNAF.

III. Physics Motivation

A. ^4He

i) Λ hypernuclei

The ^4He nucleus is one of the simplest nuclei whose wave function is obtained with the realistic interactions. In order to obtain Λ-nucleon interaction exactly, it is necessary to carry out experiments with such a nucleus for which the wave function is well known.

Experiments on Λ hypernuclear state of $^4_\Lambda H$ have been performed by the stopped K reaction[7]. The life time of the 1^+ states has been measured[8]. In the ^4He(e, e' K^+) reaction , the 1^+ state with the configuration of $(s_{1/2}^\Lambda , s_{1/2}^{-1})$ is predicted to be favorably excited, but the cross section for non spin-flip 0^+ state is smaller than that for the 1^+ state by about two orders of magnitude as shown in Fig.1[5]. As the energy difference between the 1^+ excited state and 0^+ ground state is 1.05 MeV in ^4H, the 0^+ state could be observed in the (e, e' K^+) reaction. As all the four baryons are in the orbital s-state, these two energy levels correspond directly to the Λ-N spin singlet and spin triplet states, respectively. The Λ-N spin-spin property can be investigated. Calculations[9] with five Λ-N interactions are compared in Fig. 2.

ii) Σ hypernuclei

ii) Σ hypernuclei

The Σ hypernuclear state is quite interesting, since the narrow Σ states is unanticipated because of the strong ΣN – ΛN conversion. The first evidence for the bound Σ hypernuclear state of ^{4}He has been found at a binding energy of 3.2 MeV with respect to the Σ^+ emission threshold, with a width of 4.6 MeV, via the stopped K reaction (Fig. 3)[3]. Recently clear evidence of the bound Σ hypernuclear state of ^{4}He was found in the ^{4}He(K^-, π^-) reaction at BNL[4]. In contrast to the stopped K reaction, the reaction mechanism of the in-flight (K^-, π^-) reaction is simple, so that theoretical calculations are more reliable. Also, the large background of pions from the decays of Λ and Σ is out of range in momentum. As shown in Fig. 4, the existence of the bound state was confirmed as a clear peak below the Σ–binding threshold in the ^{4}He(K^-, π^-) reaction. The width is found to be 7 ± 1 MeV. It is important to confirm the Σ hypernuclear state with other reactions, especially with the electromagnetic reaction. The electro-production is superior to the (K^-, π^-) reaction in low background and relatively reliable analysis.

Observed narrow width has been interpreted as follows by Akaishi and his collaborators[10]. A potential between Σ and a core nucleus is expressed by a central potential and the Lane term, which has isospin operators. In $^4_\Sigma$He nucleus, h+Σ^0 and t+Σ^+ channel components exist as shown in Fig. 5, the channel potentials are repulsive at short distances, while the coupling potential between the two channels is very attractive. The Lane term produces attractive potential to make a bound state. In Fig. 6 the same nucleus -Σ potential is plotted for the isospin T=1/2 and T=3/2. As seen in the figure, the potential for the T=1/2 state is attractive with slight repulsive part in the central region. On the other hand the potential for the T=3/2 state is strongly repulsive in the real part; no bound state can be realized. The energy and width predicted with the calculation are in agreement with the experimental data[3] obtained from the stopped K reaction on ^{4}He. Since the isospin of $^4_\Sigma$H can be T=1/2, it is expected to be bound. Then we want to search a bound Σ hypernuclear state through the ^{4}He(e, e' K^+) reaction.

The production cross sections for the Σ hypernucleus are estimated by Shinmura[5]. The cross section for $^4_\Sigma$H with spin = 1 is about 4 nb/sr^2/GeV at forward angle (Fig. 1).

iii) Comparison with quasifree hyperon production

In the experiments, quasifree hyperon productions are largest background process for hypernuclear productions. This background process has been estimated by Shinmura[5]. In this calculation quasifree hyperon production cross sections are given by products of the free elementary cross section, quasifree response function and kinematical factor.

include quasifree hyperon productions and hypernuclear productions. Peak widths are assumed to be 4 MeV for $^4_\Lambda$H and to be 5 MeV and 10 MeV for $^4_\Sigma$H. From Fig. 7 if the $^4_\Sigma$H exists, we can observe clearly its signal. For Λ hypernuclei, the electroproduction experiment is promising.

B. ^{3}He

i) Λ hypernuclei

The ^{3}He(e, e'K$^+$)$^3_\Lambda$H reaction is attractive because information on the nucleon hyperon interaction might be obtained explicitly using Faddeev calculations. The lightest hypernuclei $^3_\Lambda$H consists of a Λ particle weakly bound to a deuteron core. From the helium bubble chamber experiments in the K$^-$+ ^{4}He reaction[11], the production rate and the life times for two-body decays and three-body decays were measured. The binding energy of $^3_\Lambda$H was measured to be 0.25 ± 0.31 MeV. The decay branching ratio defined as the two-body decays divided by the all other pionic decays was measured to be 0.36, which is in agreement with the value calculated for spin 1/2 for $^3_\Lambda$H.

Recently Shinmura calculated the cross section for Λ hypernuclear state under the same kinematical condition as that for ^{4}He (p_e = 3.0 GeV/c, $p_{e'}$ = 1.2 GeV/c, θ_e = 6°)[12]. In the calculation the parameters of set I are used, which is determined by Hsiao and Cotanch[13]. The size of the deuteron in $^3_\Lambda$H seems to be similar to that of the deuteron in ^{3}He. The result is shown in Fig. 8. The cross section is smaller than that for the $^4_\Lambda$H (S = 1) production. The reason why the cross section reduces is due to the normalization effect by 1/10 and the spin-flip amplitude by 1/3. Then cross section for the $^3_\Lambda$H (S = 1/2) hypernuclear state is smaller than that for the $^4_\Lambda$H (S = 1) by 1/30. The $^3_\Lambda$H hypernuclear state with S = 3/2 is considered to be unbound from the theoretical interpretation, and hence it is expected to exist as a resonance. If we observe such a structure, the interaction can be determined as the wave function is exactly determined.

ii) Σ hypernuclei

The structure of A = 3 Σ hypernuclei is investigated on the basis of a central two-body ΣN interaction by Koike and Harada[14]. In $^3_\Sigma$H with S =1/2 isospin would not be a good quantum number due to the threshold energy difference and Coulomb potential. The energy and width of the $^3_\Sigma$H unstable bound state with T ≈ 1 (96 %) are obtained as $E_\Sigma{}^0$ = +0.01 MeV, Γ = 1.95 MeV for SAP-1, and $E_\Sigma{}^0$ = + 0.63 MeV, Γ = 8.20 MeV for SAP-F. Although there are no bound states, it is expected to observe the characteristic structure

due to the pole, which depends strongly on the characteristic feature of the nucleus -Σ potential.

IV. Summary of proposed measurements

We propose to measure the angular distribution of kaons produced by the (e, e' K^+) reaction on ^{3}He and ^{4}He. Incident and scattered electron energies and the kaon angles will be 3.0 and 1.2 GeV and θ=6°, 9° and 12.5°. The (e, e' K^+) measurements are not feasible anywhere but TJNAF. The data obtained will provide a test of the capabilities of the study of deeply bound states in heavy nuclei.

V. Experimental technique

i) Septum magnet

Two septum magnets will be added to the Hall A HRS2 spectrometers to allow measurements at more forwards angles (smaller than 12.5°, the minimum achievable now, up to 6°). The magnets have been designed for hypernuclear electroproduction experiments. It has been shown that it is possible to add septum magnets without major modifications of the characteristics of the spectrometers (namely the solid angle and the energy resolution). The angular acceptance will be 4.5 mrad, and the momentum resolution to < 2. x 10^{-4}. Moreover, the aim is to have a general purpose device, so particles scattered at the new minimum angle should also reach momenta as high as the maximum central momentum analyzable by the HRS2 (4 GeV/c), while keeping the possibility of varying the angle from 6° to 12.5°, the "normal" HRS setup minimum angle. In Table 1 we summarize the desired performances of the new HRS + septum spectrometer.

Physically, the first quadrupole (Q_1) of the spectrometers cannot be moved closer than 12.5° to the beam without hitting the beam pipe. So the target will be moved upstream to a suitable distance, and a horizontal-bending septum magnet will be inserted before the point element in the spectrometers in such a way that target seems to be situated on the optical axis of the two spectrometers (Figs. 9, 10). In Table 2 we summarize the dimensions of the septum. Taking into account the limited space available for the septum (about 1.5 m along the beam axis), the required aperture width, and the desired product B·l = 2.4 T–m, it can be shown that a magnet with warm coils saturates

and therefore does not satisfy the conditions. Therefore, the option of two independent iron-shaped field SC dipoles was chosen as the basic concept for the design.

A conceptual design of the septa fulfilling completely the aforementioned characteristics has been completed. In Table 3 we report the septum parameters that depend on momentum and scattering angle of detected particles. P is the scattered particle momentum, theta is the scattering angle, beta is the horizontal bending angle of the septum magnet, the magnetic field (in the region of constant field) and field integral over the path are B_0 and B·dl. R is the horizontal radius of curvature for the septum magnet. The stray field generated by the septa is shown in Fig. 11 (the center of scattering chamber is located at z > 158). Its integral along the beam pipe is 0.1T-m. To compensate the particle trajectory deflection along the beam pipe a corrector coil will be added as shown in Fig. 12. The stray field in the target region is of the order of 20 gauss, that can be easily shielded by some mm of mu metal. A request for proposals has been sent several companies . The magnets should be ordered by September '97 and installed and commissioned before the end of '98. The support structure for the magnets consists of a three-point table, with two legs supported on the HRS spectrometers and one leg using the old target pivot (for the nominal targets). The three point system is easier to level than a four-point system and provides a means of adjusting the height.

Possible source of background in the detector include neutrons, multiple scattered electrons and hadrons and "junk" created by photons and electrons from the target which interact with the pole faces of the magnet and produce a spray which is directed toward the detectors. The simplest way to control these sources of background are through shielding and baffling. The data available from Hall A commissioning suggest the shielding is adequate. Baffling is being done for this experiment actively through the use of the magnetic fields. Low energy particles are swept away by first the septum (horizontally) and then the dipole (vertically). The septum setup will therefore have reduced backgrounds compared to the normal running situation in Hall A, and there is no problem foreseen with backgrouds.

ii) Particle identification, Single rates and Accident coincidence rates

In the electron arm, pions and electrons will be separated by the gas Cherenkov and shower counters with the due rejection ratio. In the hadron arm, kaons and pions will be separated by the areogel Cherenkov counter and protons and kaons by TOF.

We are going to use Jefferson Lab cryogenic ^{3}He and ^{4}He targets of which area densities are 0.93 and 0.75 g/cm^2, respectively. Single rates for both arms and accidental coincidence rates are calculated under the following assumption;

Beam energy = 3 GeV
Beam current = 50 μA
Electron arm angle = 6°
Momentum acceptance = 10%
Angular acceptance = 4.5 msr
hadron arm momentum = 1.475 GeV/c
Coincidence time = 2 nsec

The results are shown in Tables 4-6.

The angle for outgoing kaon minimizing the momentum transfer (p_B) is examined. As shown in Fig. 13, a recoil momentum becomes minimum around 5° and is about 0.3 MeV/c. On the other hand, a final electron energy minimizing p_B, which is not clear as much as kaon angle but is around 1.1 GeV.

The counting rates for the ^{4}He(e, e' K$^+$)$^4_\Lambda$H, ^{4}He(e, e' K$^+$)$^4_\Sigma$H and ^{3}He(e, e' K$^+$)$^3_\Lambda$H reactions are estimated using the cross sections for these reactions calculated by Shinmura[4]. In this estimation the kinematical values mentioned above and a survival correction of 0.1 for kaons are assumed. The resulting count-rate estimates are shown in Table 7.

VI. Beam time request

In order to study the lambda and sigma hypernuclear states with high resolution for ^{3}He and ^{4}He targets nuclei, we request a total of 800 hrs (data acquisition : 350 hrs for angular distribution measurements at three angles in ^{4}He, 350 hrs for ^{3}He) of beam time. This includes 100 hrs of running for calibration and checkout. We think that with this beam time information on spin-spin interaction and the bound sigma hypernuclear state can be extracted.

References

[1] R. E. Chrien, Nucl. Phys. A478, 705c (1988).

[2] C. B. Dover, D. J. Millener and A. Gal, Phys. Rep. 184, 1 (1989).

[3] R. S. Hayano et al., Phys. Lett. B231, 355 (1989).

[4] T. Nagae et al., to be published in Proc. INS Symp. (1997).

[5] S. Shinmura, Prog. Theo. Phys. 92, 571 (1994).

[6] W. Hinton et al., Bull. Am. Phys. Soc. 42, 980 (1997).

[7] M. Bedjidian et al., Phys. Lett. 83B, 252 (1979).

[8] H. Outa et al., Nucl. Phys. A547, 109c (1992).

[9] T. Motoba and Y. Yamamoto, Nucl. phys. A585 29c (1995).

[10] Y. Akaishi, Perspectives of Meson Science eds. T. Yamazaki, K. Nakai and K. Nagamine (Elsevier Science publishers, 1992), p. 521.

[11] G. Keyes et al., Phys. Rev. D1, 66 (1970).

[12] S. Shinmura, private communication.

[13] S.S. Hsiao et al., Phys. Rev. C28, 1668 (1983).

[14] Y. Koike and T. Harada, Nucl. Phys. A611, 461 (1996).

[15] A Proposal for Two Septum Magnets for Forward Angle Physics in Hall A at TJNAF.

Table 1. Performance Requirements.

	HRS	HRS(a)	Septum	Septum(r)
Angular acceptance	7.3 msr	6 msr	4.5 msr	3.7 msr
Momentum resolution	1.0×10^{-4}	2.0×10^{-4}	1.0×10^{-4}	2.0×10^{-4}
Minimum scattering angle	12.5°	12.5°	6°	6°
Momentum range	0.4 - 4 GeV/c	0.4 - 4 GeV/c	0.4 - 4 GeV/c	0.4 - 4 GeV/c

HRS (a) : HRS presently achieved performances

Septum(r) : consequent implied realistic performances

Table 2. Septum Dimensions.

Length *	88. cm
Height of the gap	25. cm
Width of gap entrance edge	10.4 cm
Width of gap exit edge	18.4 cm
Angular acceptance	4.7 msr
Magnetic length	84. cm

(*length includes length of the coils outside the yoke)

Table 3. Septum Parameters.

P GeV/c	θ degrees	β degrees	R cm	B·dl Tesla-m	B_0 Tesla
2	6	6.5	740.8	0.76	0.9
2	12.5	11.9	404.6	1.39	1.65
4	6	6.5	740.8	1.51	1.8
4	12.5	11.9	404.6	2.89	3.3

Table 4. Electron Arm Single Rates.

Target	Particle	Rates (kHz)
^{4}He	e	1700
^{4}He	π^-	614
^{3}He	e	2230
^{3}He	π^-	737

Table 5. Hadron Arm Single Rates.

Target	Particle	Angle 6° Rates (kHz)	9° Rates (kHz)	12.5° Rates (kHz)
^{4}He	p	129	114	94
^{4}He	π^+	450	304	182
^{3}He	e	142	125	102
^{3}He	π^+	574	389	232

Table 6. Accidental Coincidence Rates.

Target	Coincidence Particle	Angle 6° R_{Coin} (Hz)	9° R_{Coin} (Hz)	12.5° R_{Coin} (Hz)
^{4}He	e - p	436	388	320
^{4}He	e - π^+	1530	1033	616
^{3}He	e - p	632	559	456
^{3}He	e - π^+	2561	1732	1042

Table 7. Count Rate Estimates.

Target	E_e (GeV)	$E_{e'}$ (GeV)	$\vartheta_{e'}$	ϑ_K	P_K (Λ state) (GeV/c)	P_K (Σ state) (GeV/c)	Cross Section (nb/sr^2/GeV)		Rates /hr	
							Λ	Σ	Λ	Σ
^{4}He	3.0	1.2	6°	6°	1.514	1.421	4.2	6.0	130	190
^{4}He	3.0	1.2	6°	9°	1.511	1.419	2.1	4.6	65	140
^{4}He	3.0	1.2	6°	12.5°	1.506	1.413	0.75	2.5	23	77
^{3}He	3.0	1.2	6°	6°	1.525	1.428	0.047		2.40	
^{3}He	3.0	1.2	6°	9°	1.521	1.424	0.013		0.66	
^{3}He	3.0	1.2	6°	12.5°	1.514	1.417	0.0022		0.11	

Cross sections and count-rate estimates are shown for $^4_\Lambda$H($J_f = 1$), $^4_\Sigma$H ($J_f = 1$) and $^3_\Lambda$H ($J_f = 1/2$).

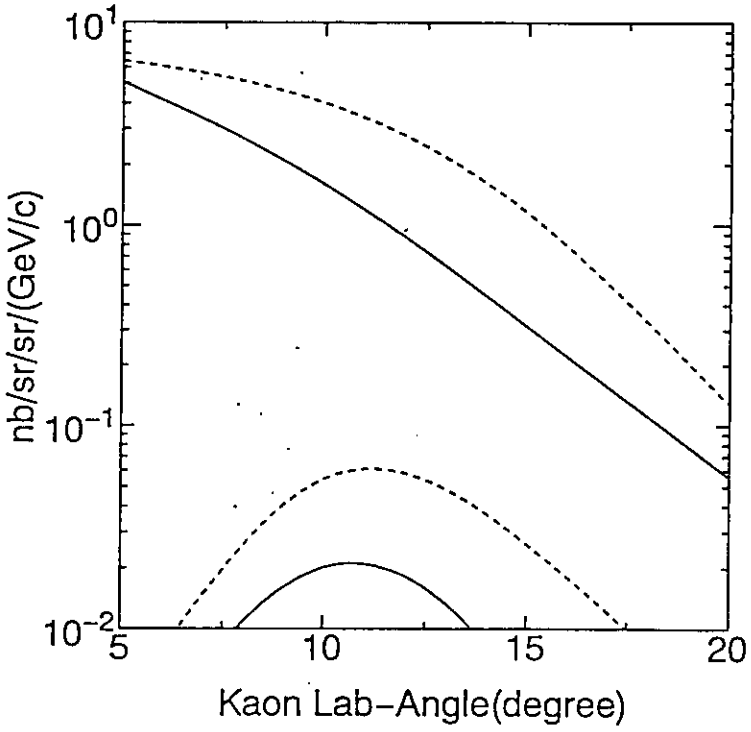

Fig. 1. Angular distributions of ^{4}He(e, e' K^{+})$^{4}_{\Lambda}$H, $^{4}_{\Lambda}$H*, $^{4}_{\Sigma}$H and $^{4}_{\Sigma}$H*, which correspond to lower solid, upper solid, lower dotted and upper dotted lines, respectively; p_e = 3.0 GeV/c, $p_{e'}$ = 1.2 GeV/c, $q_{e'}$ = 6° (ref. 5).

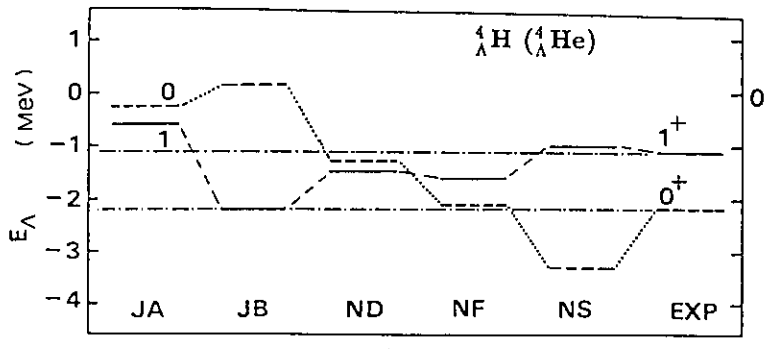

Fig. 2. Energy levels of $^{4}_{\Lambda}$H($^{4}_{\Lambda}$He), 0^{+}(dashed) and 1^{+}(solid), as calculated in the generator coodinate method (ref. 9).

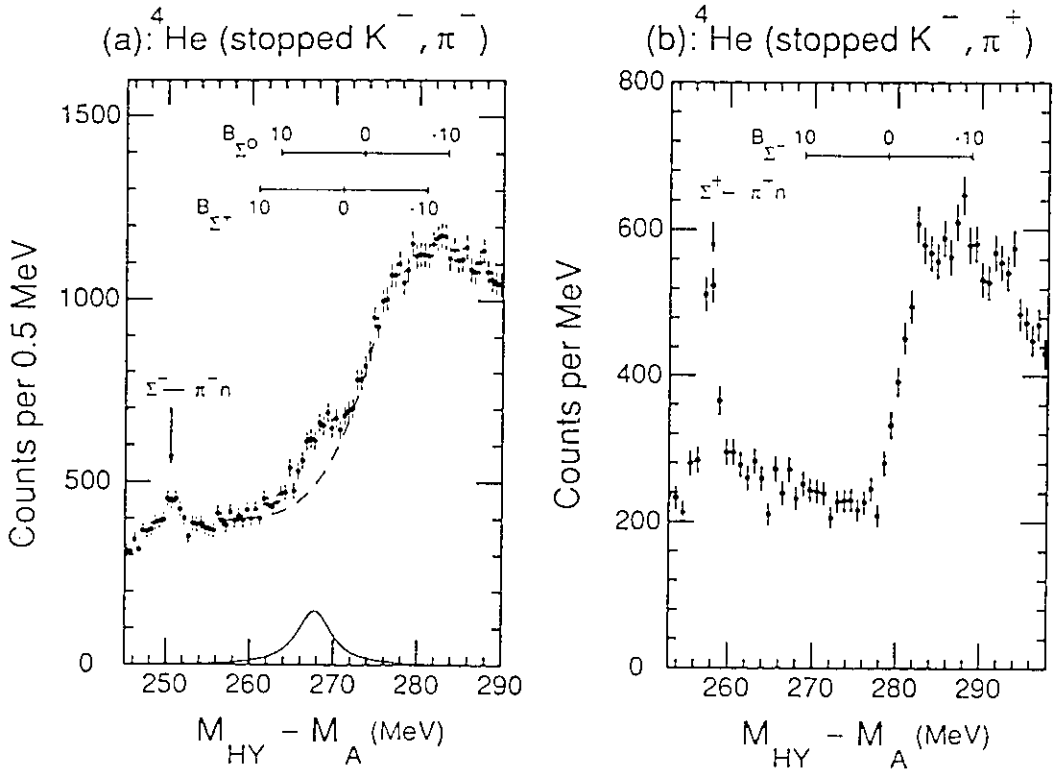

Fig. 3. a) The π^- spectrum plotted in the hypernuclear mass scale, M($^4_\Sigma$He)-M(^{4}He). Binding energy scales for Σ^+ and Σ^0 are indicated in the figure. b) The π^+ spectrum observed in the (K^-,π^+) reaction at rest on a herium target, shown in the hypernuclear mass scale (ref. 4).

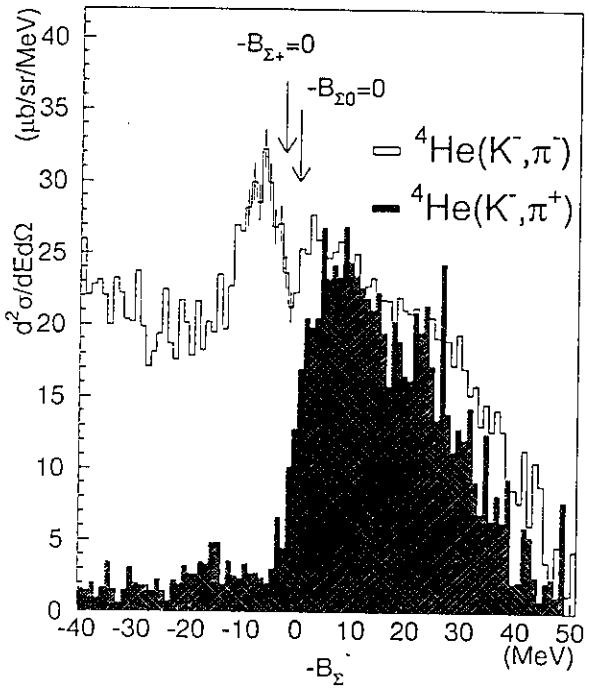

Fig. 4. Spectra of the ^{4}He(K^-, π^+) reactions at p_K = 600 MeV/c, θ = 4° obtained in E905. A clear peak is found in the bound region only in the ^{4}He(K^-, π^-) spectrum.

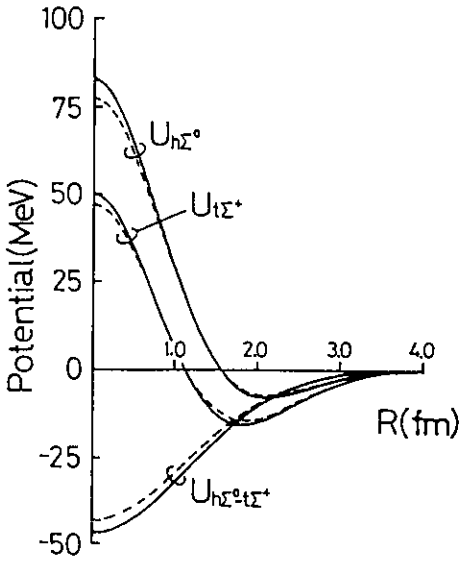

Fig. 5. The real part of the nucleus-Σ channel and coupling potentials. The potentials of the $^3H+\Sigma^+$ and $^3He+\Sigma^0$ channels are denoted by $U_{t\Sigma+}$ and $U_{h\Sigma0}$ and the coupling potential by $U_{h\Sigma0-t\Sigma+}$. The solid and the dashed curves are for different sigma absorption potentials (ref. 10).

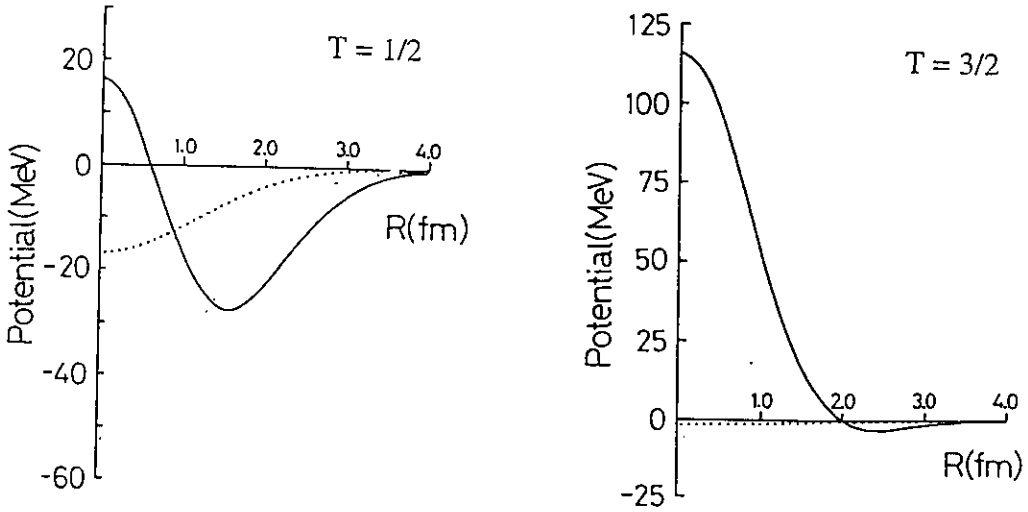

Fig. 6. The nucleus-Σ potentials for the isospin T=1/2 and T=3/2 states. The solid and the dotted lines are the real and the imaginary parts, respectively (ref. 10).

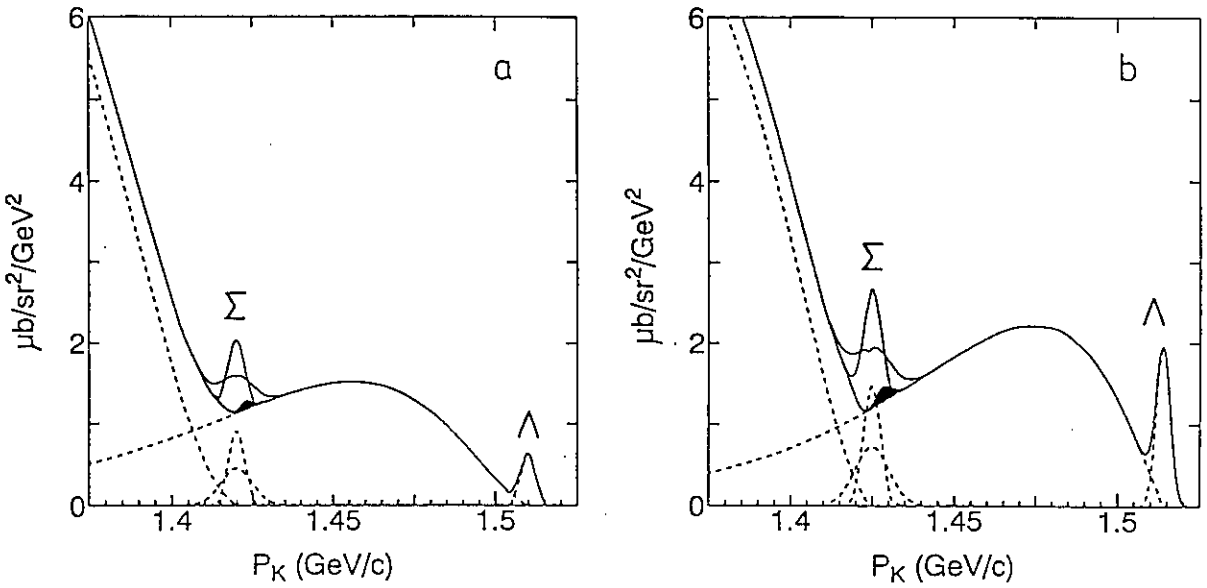

Fig. 7. Predicted spectra including quasifree hyperon productions and hypernuclear productions in ^{4}He(e, e' K$^+$)X at $\theta_K = 10^\circ$ (a) and 5° (b). Peaks labeled Λ and Σ are $^4_\Lambda$H* ($\Gamma = 4$ MeV) and $^4_\Sigma$H* ($\Gamma = 5$ MeV and 10 MeV) productions, respectively. Filled peaks correspond to 10 % of $^4_\Lambda$H* ($\Gamma = 5$ MeV) peaks (shifted to the $B_\Sigma = 5.1$ MeV for $^{16}_\Sigma$N) (ref. 5).

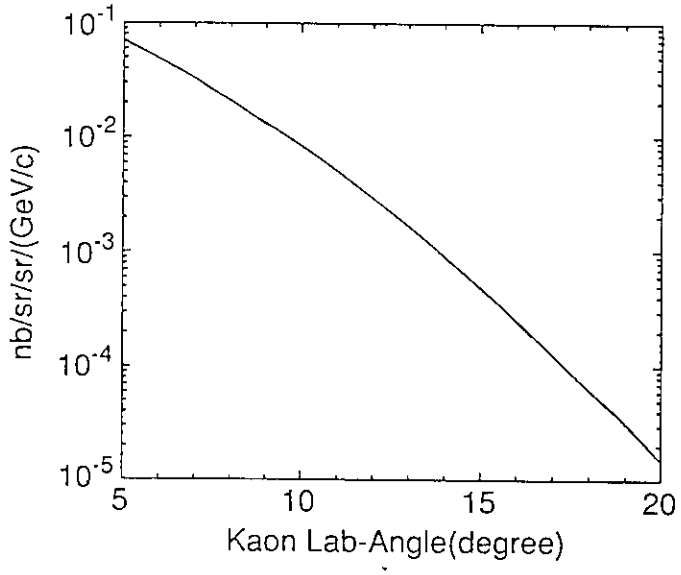

Fig. 8. Angular distributions of ^{3}He(e, e' K$^+$)$^3_\Lambda$H. $p_e = 3.0$ GeV/c, $p_{e'} = 1.2$ GeV/c, $\theta_{e'} = 6^\circ$ (ref. 12).

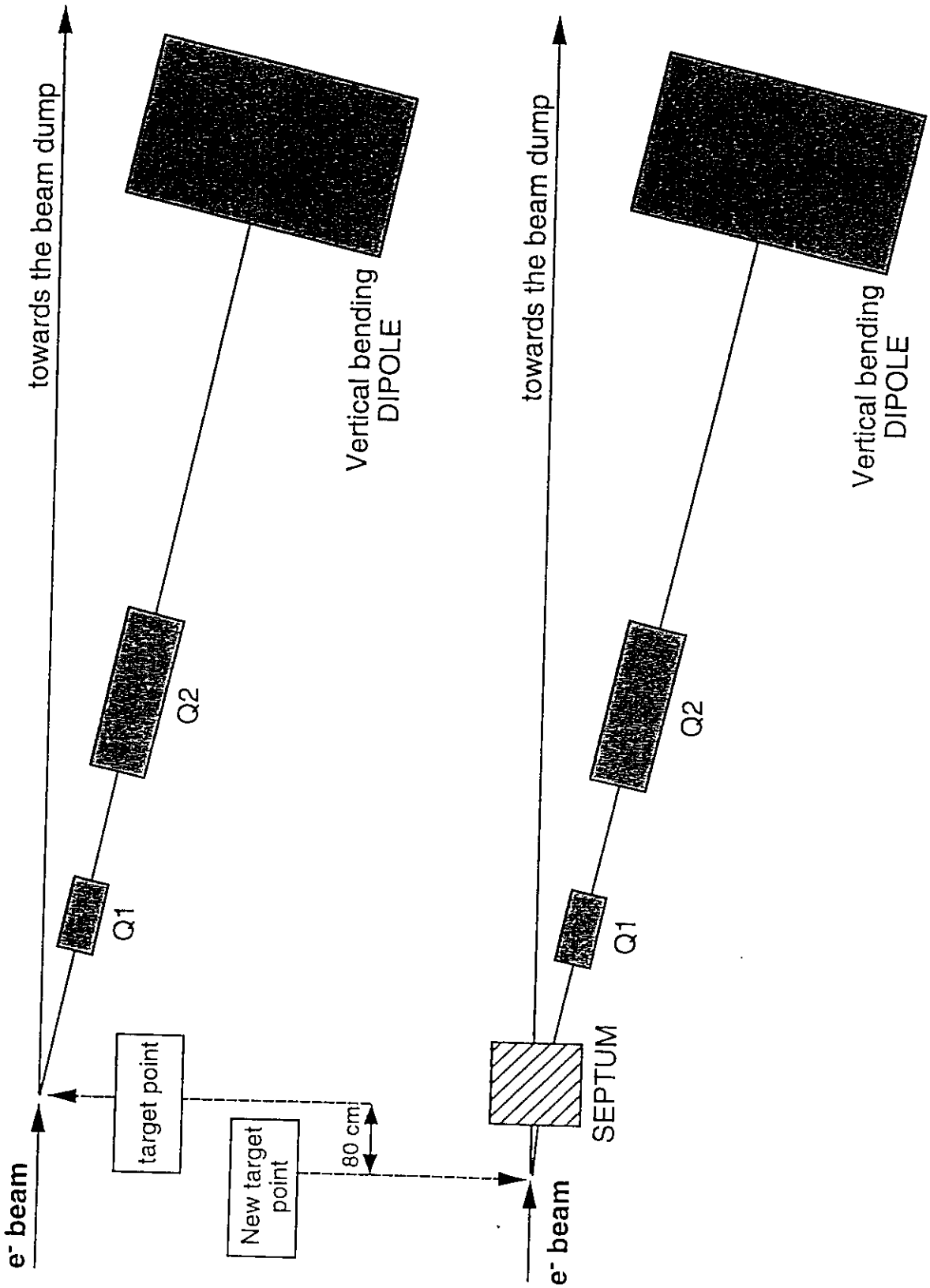

Fig. 9. Schematic layout of the proposed modifications to the HRS set up.

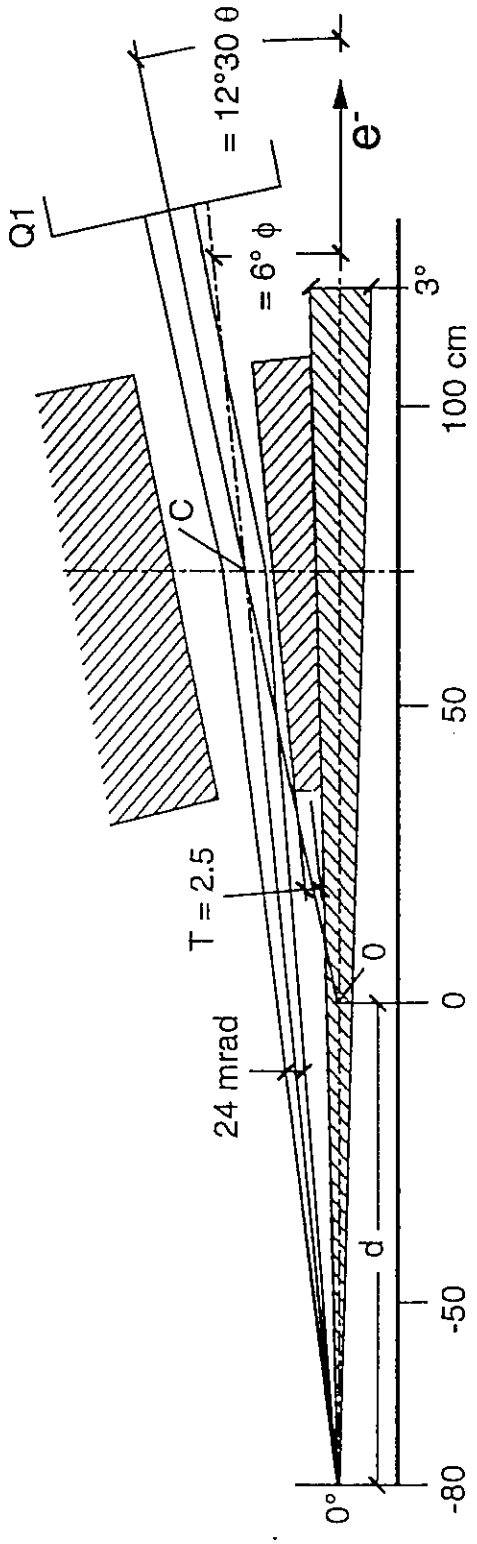

Fig.10. Layout of the septum insertion.

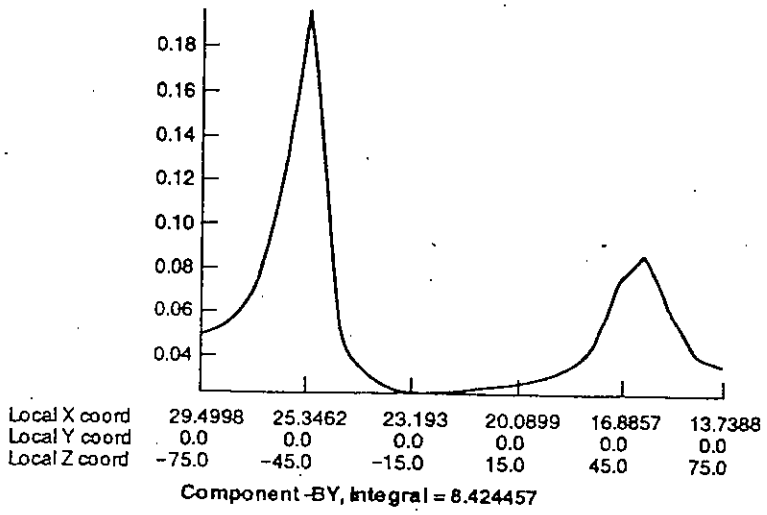

Fig. 11. Stray field generated on the beam pipe in the case 6°.

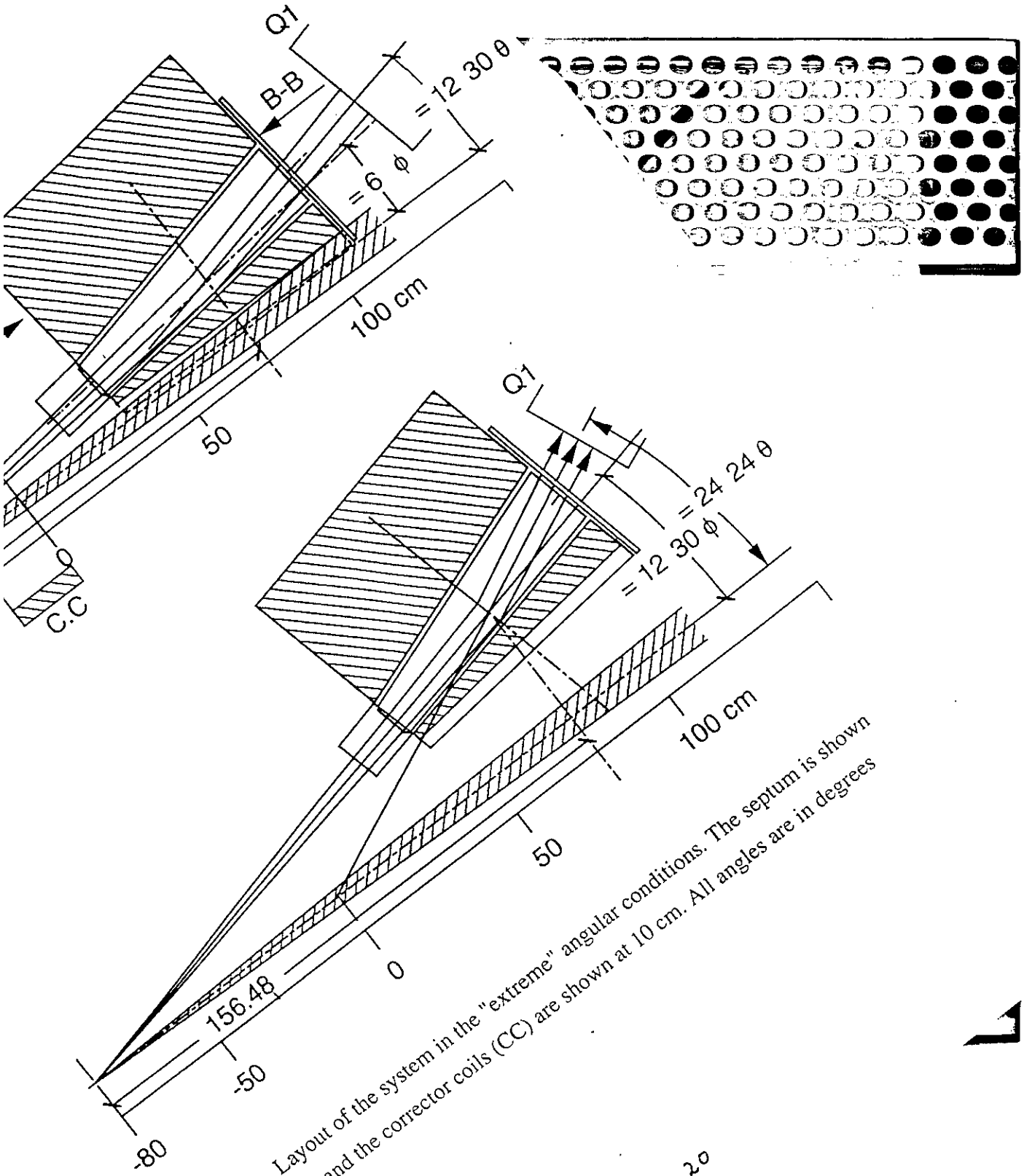

Fig. 12. Layout of the system in the "extreme" angular conditions. The septum is shown at 70 cm and the corrector coils (CC) are shown at 10 cm. All angles are in degrees and minutes.

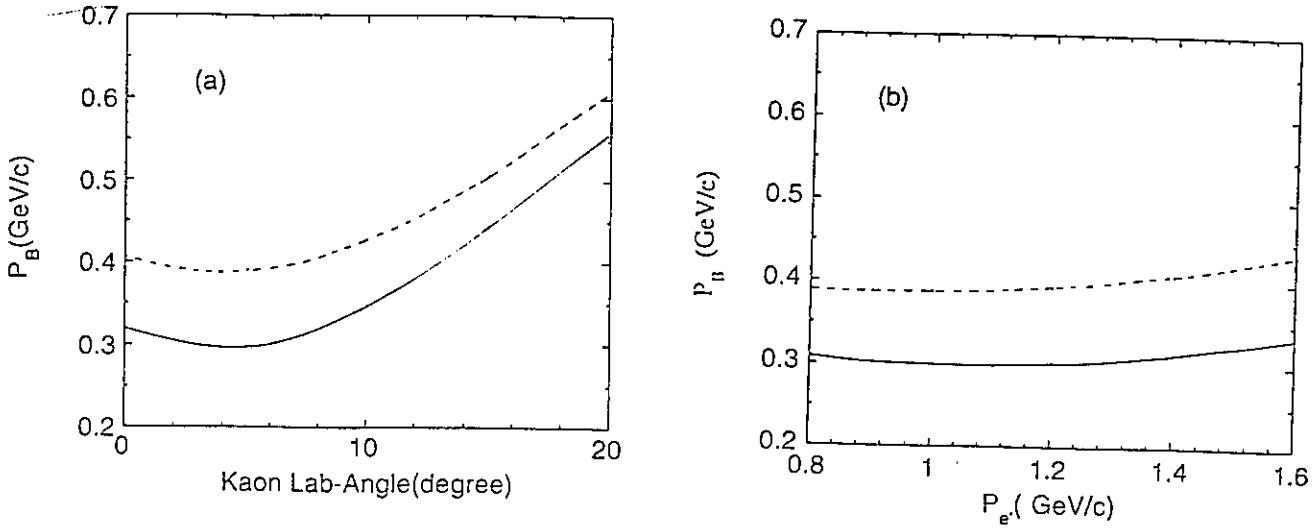

Fig. 13 Momentum transfer to hypernuclei as a function of K^+ angle, θ_K (a) and final electron momentum, $p_{e'}$ (b) in the case of ^{4}He(e, e'K^+). In the figures solid and dotted lines are the cases with $^4_\Lambda$He and $^4_\Sigma$He, respectively.